Miscible viscous fingering in three dimensions: Fractal-to-compact crossover and interfacial roughness

M. Ferer,[1,2] Grant S. Bromhal,[2] and Duane H. Smith[1,2]
[1]*Department of Physics, West Virginia University, Morgantown, West Virginia 26506-6315, USA*
[2]*US DOE–National Energy Technology Laboratory, Morgantown, West Virginia 26505-0880, USA*
(Received 24 October 2008; revised manuscript received 3 April 2009; published 8 July 2009)

Using our standard pore-level model, we have extended our earlier study of the crossover from fractal viscous fingering to compact /linear flow at a characteristic crossover time, τ, in three dimensions to systems with as many as a 10^6 pore bodies. These larger systems enable us to investigate the flows in the fully compact/well-past-crossover regime. The center of mass of the injected fluid exhibits basically the same behavior as found earlier but with an improved characteristic time. However, our earlier study of much smaller systems was unable to study the interfacial width in the important well-past-crossover regime, $t \gg \tau$. Now, we can study both the time evolution and roughness of the interfacial width. The interfacial width exhibits the same fractal-to-compact crossover as the center of mass, with the same characteristic time. In the fully compact regime, $t \gg \tau$, the interfacial width grows approximately linearly with time so that the standard growth exponent is approximately unity, $\beta = 1.0 \pm 0.1$. We find that neither is the interface self-affine nor is the roughness of the interface in the compact regime consistent with an effective long-range surface tension as assumed by various theories. In fact, similar to Lévy flights, the height variations across the interface appear to be random with occasional large height variations.

DOI: 10.1103/PhysRevE.80.011602 PACS number(s): 68.05.−n, 47.56.+r, 47.53.+n

I. INTRODUCTION

A. Fractal-to-compact crossover

Over twenty years ago, it was shown that this average position (center of mass) of the injected fluid (a measure of the interfacial position for compact flows) was not linearly related to the amount of injected fluid if the injected fluid had a viscosity very much smaller than the viscosity of the defending fluid, i.e., for near-zero viscosity ratio,

$$M = \frac{\mu_i}{\mu_d} \approx 0, \tag{1}$$

where μ_i and μ_d are the viscosities of the invading and defending fluids, respectively [1]. Theoretical arguments and comparisons with experiment showed that flows for this case of negligible viscosity ratio could be described by the diffusion-limited-aggregation (DLA) model, for which the fractal dimension is approximately $D_f \approx 1.71$ in two dimensions ($d=2$) and $D_f \approx 2.5$ for $d=3$ [2–6]. For constant injection rate in the vertical x direction, the mass or volume of the incompressible fluid is proportional to time, which is defined in terms of the total amount of injected fluid, V,

$$t = V/A, \tag{2}$$

where A is the area of the base through which the invading fluid is injected so that time t is essentially the total saturation multiplied by the height H of the system. Therefore, the fractal behavior of DLA predicts that a typical length scale, e.g., the average position of the injected fluid, is related to the injected fluid volume or time via the nonlinear fractal relation

$$\langle x \rangle \propto t^{1+\varepsilon}, \tag{3}$$

where [4]

$$1 + \varepsilon = \frac{1}{D_f - (d-1)} \approx \begin{cases} 1.4, & \text{for } d = 2 \\ 2.0, & \text{for } d = 3 \end{cases}. \tag{4}$$

In earlier publications, we first addressed the discrepancy between the standard practice, which assumes compact flow with a linear relationship between the average position and the amount of injected fluid, and the nonlinear or fractal relationship that is valid for very small-viscosity ratios [7–9].

Our modeling results showed that the initial fractal flows would start to become compact at a characteristic time, which varied inversely with viscosity ratio,

$$\tau \propto M^{-p}, \tag{5}$$

where the value of the power, which best represented our modeling data for a wide range of viscosity ratios in two dimensions, is given by $p=0.17$ [8]. We also had results for three-dimensional (3D) systems that showed the same crossover behavior with a value of the exponent p in the range $p \approx 0.16$–0.21 [7]. At that time, computer resources limited our $d=3$ modeling to systems with 125 000 pore bodies ($50 \times 50 \times 50$) for which the linear size (50) was too small to exhibit fully compact behavior; hence the uncertainty in the value of p. Recently, we have performed simulations on systems with as many as a 10^6 pore bodies ($100 \times 100 \times 100$), which are large enough to exhibit well past crossover, i.e., fully compact behavior. In this paper, we show that our fractal-to-compact crossover naturally leads to a compact limit where a simple power law, as in Eq. (5), effectively represents the important large time behavior.

B. Interfacial roughness

There have been many studies of surface roughness, investigating not only the roughness of the interface between the two fluids flowing in two-dimensional (2D) porous media

[9–15], but also the roughness of fracture surfaces [16–19]. The majority of studies of two fluid flow in porous media focused on flows with marginally stable interfaces, i.e., rough but not dramatically unstable interfaces: e.g., imbibition [11,12], and gravity stabilized flows [13]. These marginally stable interfaces in the flows are often found to be self-affine and are characterized by the interfacial widths averaged over a length scale L (i.e., all $L\times L$ regions perpendicular to the average flow) as a function of time t. The functional dependence of this width was often found to obey a homogenous function

$$\langle w(t,L)\rangle = t^{\beta} g(t/L^{\alpha/\beta}) = L^{\alpha} f(t/L^{\alpha/\beta}), \tag{6}$$

so that $\langle w(t,L)\rangle = f(\infty)L^{\alpha}$ for small L while $\langle w(t,L)\rangle = g(0)t^{\beta}$ for large L. In Eq. (6) β is the growth exponent and α is the roughness exponent, which is often represented by χ while the ratio α/β is often represented by z. A theory for predicting the interfacial roughness for the fluid flow case was proposed by Kardar, Parisi, and Zhang (KPZ) [10,20,21]. This theory produces results consistent with Eqs. (6) and (7), and predicts values of these exponents. A careful imbibition experiment with stable viscosity ratios in two spatial dimensions found the values $\alpha \approx 0.81$ and $\beta \approx 0.65$ [10,11], which obey the predicted scaling relation [22]

$$\alpha + \alpha/\beta = \chi + z = 2. \tag{7}$$

Our earlier pore-level modeling of unstable flow in two dimensions also found self-affine interfaces with exponents consistent with this experiment [9]. Although both this 2D experiment [10,11] and our 2D pore-level modeling [9] produced results consistent with Eqs. (6) and (7), it should be noted that these exponents were different from those 2D KPZ results with which we are familiar [21]. Furthermore, recent two-dimensional imbibition experiments exhibited behavior different from this standard picture in that the behavior is not as simple as Eqs. (6) and (7) would suggest [12]. As we will show in Sec. III, the unstable interfaces studied in this work seem to exhibit a totally random behavior rather than self-affinity so that the 3D unstable interfaces studied do not agree with KPZ or with the scaling relation in Eq. (7).

II. FRACTAL-TO-COMPACT CROSSOVER IN THREE DIMENSIONS

A. Average position of the injected fluid

Our simulations were performed using essentially the same computer code described in our earlier publications, which assumes Darcy flow in each throat and no mixing at the interface [7]. Our simple model of the porous medium consists of spherical pore bodies at the sites of a simple-cubic lattice with cylindrical throats of randomly chosen cross-sectional area connecting any one pore body to each of the six adjacent pore bodies. The length of each throat is ℓ, which defines the length scale of the porous medium; the volume in each pore body is $V=\ell^3$; the randomly chosen cross-sectional area of the throats varies between 0 and ℓ^2. Given these sizes, the diameter of each pore body is 1.24 ℓ; therefore, the pore body centers are $d=2.24\ell$ apart so that all distances are given in units of d. The model porous media used in these simulations are rectangular in shape with a height spanned by H pore bodies of length 2.24 ℓ in the x direction and a square base in the $y=z$ plane, consisting of W^2 pore bodies with total area $(W2.24\ell)^2$. In this work, most of the model porous media have shapes which are $H=100$ pore bodies high with a base of $W\times W=100\times 100$ pore bodies, consisting of a total of 10^6 pore bodies, compared to our earlier work on systems with $W=H=50$ consisting of 125 000 pore bodies. Periodic boundary conditions are imposed at the sides of the $H\times W\times W$ solid. The lower viscosity fluid is injected uniformly through the W^2 throats in the $x=0$ base; the higher viscosity displaced fluid flows out of the W^2 throats at the top. Although the terms "bottom," "top," and "vertical" are used, gravity is not included in the model in order to focus solely on the effects of viscosity ratio.

The definition of time, $t=V/A$ [Eq. (2)], used in this work can be determined from the volume of injected fluid V in units of ℓ^3 and where the area A (units of ℓ^2) is the total area of all of the throats in the base of the porous medium through which fluid is injected. Although this definition of time is effectively nondimensional, it is directly proportional to physical time t_p in seconds for constant injection rate q since $V=qt$. Examples of crossover for several flow cell experiments in the open literature were presented in Ref. [23], where we estimated when the crossover would occur in these experiments.

For three viscosity ratios, the Fig. 1 presents three-dimensional plots of the near-breakthrough flows, showing the qualitative changes on going from fractal viscous fingering to compact flow. To study the crossover, it is necessary to investigate the time dependence of the flows. For this purpose, we have generated data for the average position of the injected fluid, $\langle x\rangle$; the data shown in Fig. 2 represent this averaged over ten realizations (different random number seeds to generate the cross-sectional areas of the throats) of the porous medium structure. In the fractal limit, $\langle x\rangle$ increases with injected volume (proportional to time for constant injection) according to the power law in Eq. (3) while in the compact limit it is linearly related to injected volume or time. Figure 2 shows that $\langle x\rangle/t$ is growing as t^{ε}, where $\varepsilon=1$ [Eqs. (2) and (3)] for small times and viscosity ratios, but that $\langle x\rangle/t$ becomes constant for larger times and viscosity ratios. Therefore, the average position is "crossing over" from fractal flow to compact flow at a characteristic time, τ, which decreases as viscosity ratio increases.

In our earlier studies of miscible crossover, we showed that a successful determination of the viscosity ratio dependence of the characteristic time could be used to collapse all of the data to one curve, given by the function

$$\langle x\rangle = t^{1+\varepsilon} X(t/\tau), \tag{8}$$

where $\langle x\rangle = t^{1+\varepsilon}X(0)$ in the fractal limit, $t \ll \tau$ [7–9]. In the compact well-past-crossover limit, where $\langle x\rangle = vt$, the function in Eq. (8) must have the limiting form $\lim_{t\gg\tau} X(t/\tau) \rightarrow B(t/\tau)^{-\varepsilon}$ to assure the linear time dependence (B is an undetermined constant). Since Eq. (8) incorporates all of the viscosity ratio dependence, it becomes $\langle x\rangle = (B\tau^{\varepsilon})t$ in the

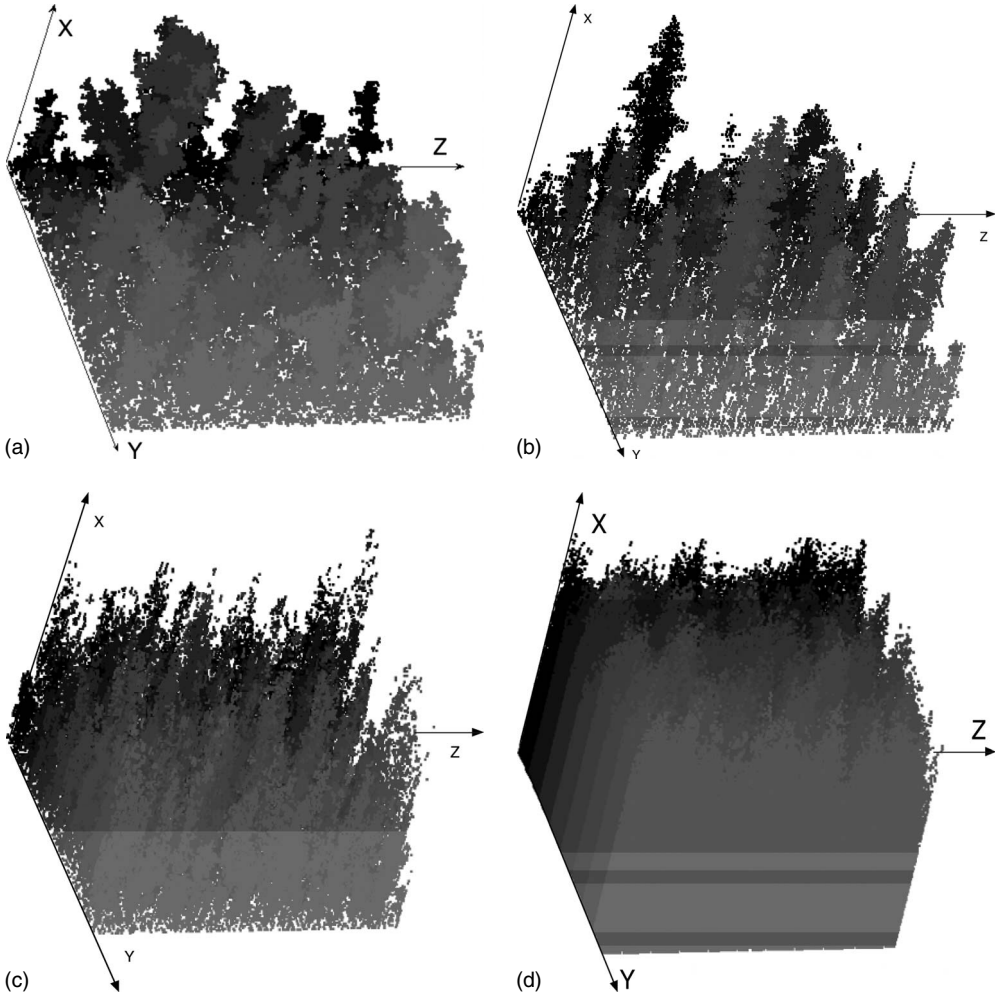

FIG. 1. Near breakthrough flow patterns are shown for (a) DLA, (b) $M=10^{-4}$, (c) $M=10^{-3}$, and (d) $M=0.1$. The gray scale shading along the y axis is intended to clarify the variations in the y direction. These figures show average flow in the x direction for our 10^6 pore body $100\times100\times100$ systems.

compact regime, thereby predicting the viscosity ratio dependence of the front velocity, $v=B\tau^{\varepsilon}$.

Following this same approach for the data in Fig. 2, Fig. 3 shows a log-log plot of $\langle x\rangle/t^{1+\varepsilon}$ vs t, where the fractal behavior is represented by a constant. Flows for the larger viscosity ratios begin by following the fractal behavior and then cross over to compact behavior following a $t^{-\varepsilon}=1/t$ time dependence in this figure.

Using the same form of the scaling variable used in our earlier publications [7–9], we find that a successful collapse of these data requires using a smaller value of the exponent p in Eq. (5) than that used in our early work studying smaller systems [7]. The correction, i.e., $6/\tau$, to the leading singularity only serves to improve the collapse in the intermediate time regime, $(t+6/\tau)/\tau\approx7$. Even for the largest viscosity ratios, this "correction term" shifting the time origin is a relatively small correction with negligible effect on the important long-time behavior, which is dominated by the leading behavior, t/τ.

B. Interfacial width

Having systems that exhibit well-past-crossover behavior for several viscosity ratios, we are now able to investigate not only the crossover of the interfacial width but also its roughness and limiting temporal behavior. We determined the interfacial width from the first, $\langle x\rangle$, and second, $\langle x^2\rangle$, moments of the injected fluid using a method presented in an earlier paper [9]. Later we will see that the temporal dependence obtained from this data is the same as the temporal dependence determined using other methods to evaluate the mean-square deviation in the interfacial position. Since interfacial width is a typical length scale, for fractal flow, the interfacial width should depend on time in the same way as the average position [6] [Eq. (4)] so that in three dimensions,

$$w_{\mathrm{DLA}}\propto t^{2.0}. \tag{9}$$

Figure 5 shows the interfacial width divided by the fractal time dependence. As expected, the small-viscosity-ratio dependence of the interfacial width obeys Eq. (9). As was observed for the average position, this crosses over from the small-time small-viscosity-ratio fractal behavior to the long-time large-viscosity-ratio behavior associated with compact flow.

Figure 5 for the interfacial width $\langle w\rangle$ corresponds to Fig. 3 for average position. Comparing Figs. 3 and 5, it is obvious

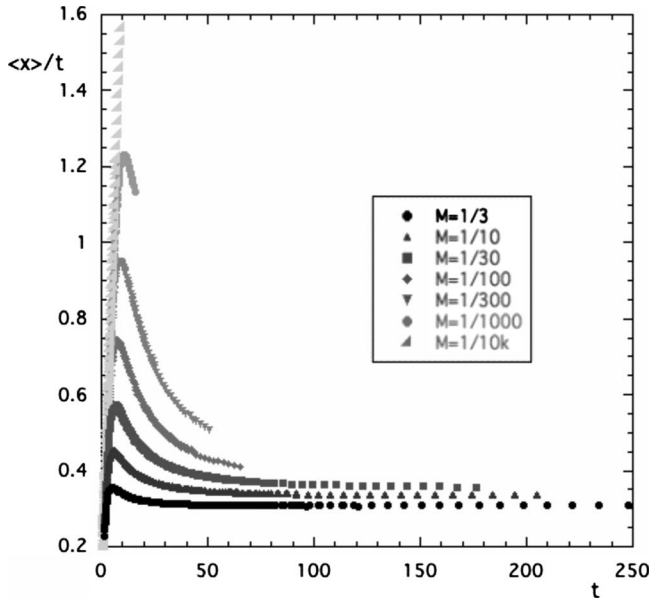

FIG. 2. The average position divided by t is plotted vs t. Data are shown for several sizes and several viscosity ratios with the plot symbols fading from black to light gray as the viscosity ratio decreases. The average position exhibits the t^2 dependence of fractal flow for short times, and then crosses over to the linear time dependence of compact flow for longer times and larger viscosity ratios. As discussed in Sec. II A, time is essentially dimensionless and distances are in units of $d=2.24\ell$.

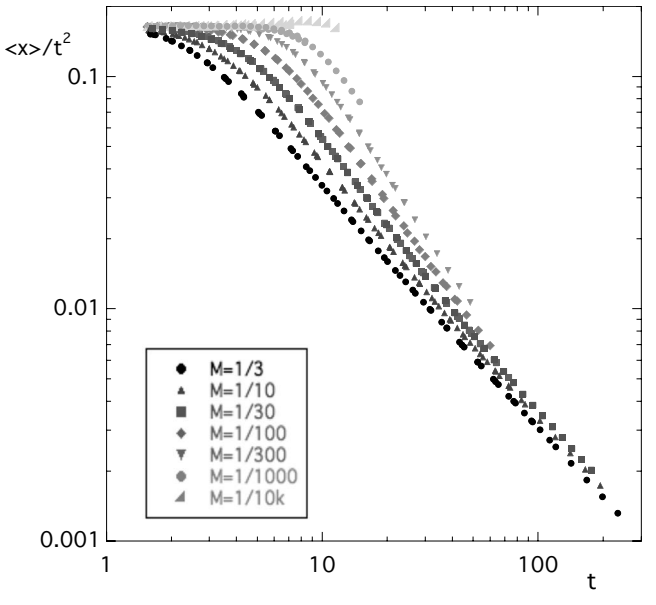

FIG. 3. $\langle x\rangle/t^{1+\varepsilon}$ is plotted vs t for the data from Fig. 2, using the same plot symbols. In practice, Eq. (2) was modified slightly by changing the time origin, $t=t_0+V/A$, for all of this data $t_0=1$. This value is a fitting parameter chosen so that the $M=1/10k$ data have the correct fractal time dependence for the smallest values of t possible. This small shift in the time origin has no effect on the important large t behavior. Also, in an earlier paper, we showed that this could arise from the differences between a discrete and a continuous model [8].

that the behavior of the interfacial width data for $M=1/3$ (filled black circles) is further below the data for other viscosity ratios than it was for the case of average position. Still, if the fractal-to-compact crossover is a feature of the flow and not just of the average position, one would expect that the same characteristic time, which accounts for the viscosity ratio dependence of the average position, would also account for the viscosity ratio dependence of the interfacial width. In Fig. 6, we plot the data from Fig. 5 with the same characteristic time used in Fig. 4.

As expected from Fig. 5, the single power in the power-law characteristic time does not correctly account for the viscosity ratio dependence of the $M=1/3$ data; there also appear to be much smaller deviations for the $M=1/10$ data (dark gray filled isosceles triangles) in that they sit slightly below the other data. This does not mean that the power-law form is invalid. Rather it suggests that this power-law form is incomplete, in that higher-order corrections to the leading singularity, $M^{-0.08}$, in the power-law form are necessary to account for the viscosity ratio dependence of the interfacial width for these largest viscosity ratios. In addition to possible higher-order nonanalytic corrections, there will certainly be analytic corrections to the leading singularity so that the characteristic time might have the form, $\tau=M^{-0.08}+cM$. Since the leading singularity does more accurately account for the viscosity ratio dependence of the data for smaller viscosity ratios, the higher-order corrections, e.g., cM, to the leading singularity, e.g., cM, must be negligible for these smaller viscosity ratios. Furthermore, although we expect the exponent of the leading singularity to be universal based on our experience from this and earlier studies [8,24], e.g., the same for different porous media structures as well as for other properties associated with the flow, we do not expect constants such as c to be universal. Therefore, even though these higher-order corrections are insignificant for the aver-

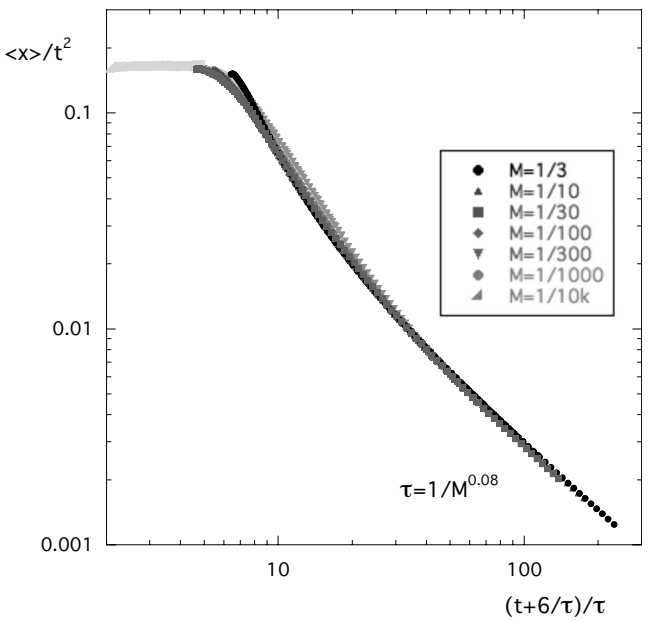

FIG. 4. The data from Fig. 2 are plotted vs a scaled time similar to that in our earlier publications [7].

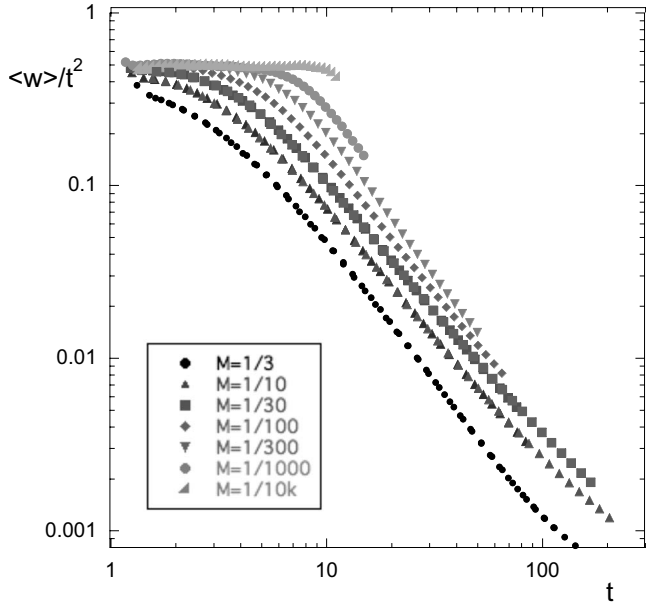

FIG. 5. The average value of interfacial width plotted vs time so that the fractal behavior is a constant. The data were determined from the same computer runs that provided the data for average position studied in Sec. II. The plot symbols are the same as those used in Sec. II.

age position in the $M=1/3$ flows, one should not necessarily expect them to be insignificant for the interfacial width of the injected fluid in the $M=1/3$ flows.

III. INTERFACIAL ROUGHNESS IN THREE DIMENSIONS

To study the interfacial width in three dimensions, let us first use the data in Figs. 5 and 6 to determine the growth

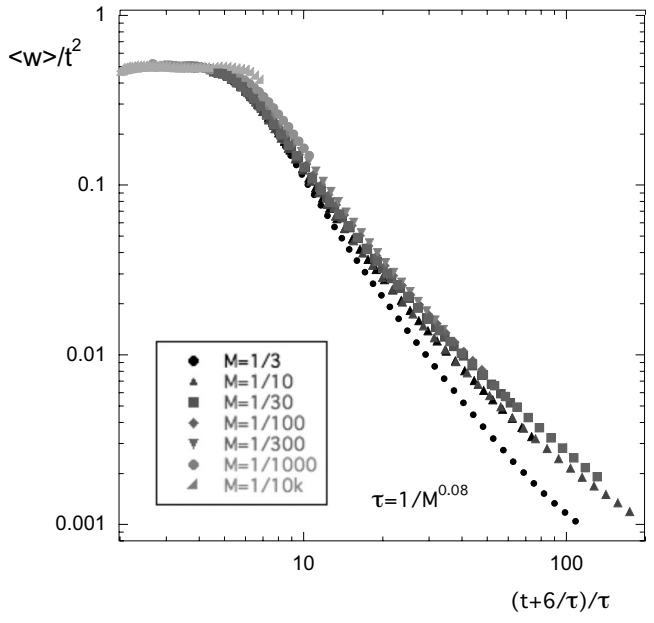

FIG. 6. The data for the interfacial width from Fig. 10 are plotted vs scaled time, which successfully collapsed the date for average position in Figs. 4 and 9.

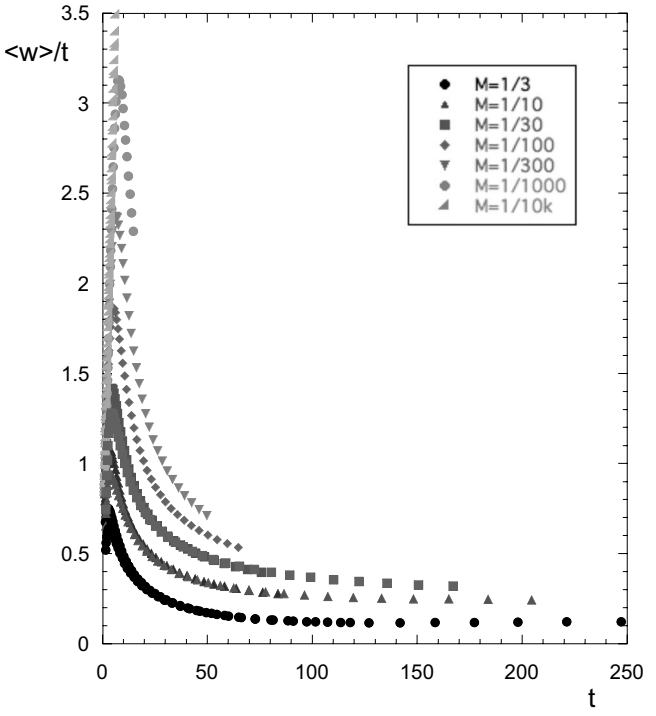

FIG. 7. The data from Figs. 5 and 6 are plotted as $\langle w\rangle/t$ vs t to demonstrate the near linear time dependence of the well-past-crossover interfacial width.

exponent. Figure 2 indicates that the data for the average position have achieved linear advance for $t>80$ for viscosity ratios, $M\geq 1/30$. Fits to the well-past-crossover data ($t>80$ and $M\geq 1/30$) in Figs. 5 and 6 indicate that the interfacial width is increasing approximately linearly with time, $\langle w\rangle=Ct$. Since this is the large L limit of Eq. (6), the near linearity of this data implies $\beta=1.0\pm 0.1$. This is demonstrated in Fig. 7, where the data for interfacial width are divided by time, $\langle w\rangle/t$. Plotted in this way, the data are approximately constant, $\langle w\rangle/t=C$, in the well-past-crossover regime.

If $\beta=1$, then the scaling relation in Eq. (7) predicts that the roughness exponent should also have the value unity, $\alpha=1$. To determine the roughness exponent from our results, we study both the near-neighbor height-height correlations and the interfacial width averaged over an $L\times L$ area of the model, which is perpendicular to the average flow direction. In studying the roughness of a surface, which has overhangs and/or disconnected ganglia of injected fluid, one conventional method of determining the height h of injected fluid above a point (j,k) in the basal plane is to use the maximum height ($h_{\max}$) that the injected fluid has attained. If one allowed for real mixing due to dispersion, then this maximum height determined from our nonmixing model would still be the greatest height that the injected fluid has attained [13]. This definition is illustrated in Fig. 8.

In looking at these height variations across this maximal surface of the injected fluid, one issue of real interest is the probability of having a certain height change, $\pm\Delta h_1$, by taking a single nearest-neighbor (nn) step parallel to the basal plane, i.e., from any (j,k) to either $(j\pm 1,k)$ or $(j,k\pm 1)$. Of course, height differences $+\Delta h_1$ and $-\Delta h_1$ are equiprobable

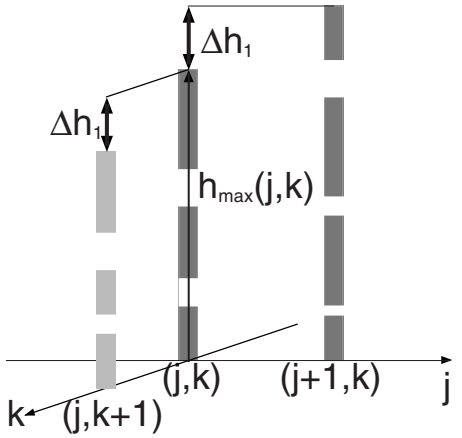

FIG. 8. The figure shows a 3D cartoon representation of three typical injection sites in the $(y,z)=(j,k)$ basal plane with occupation solely along the columns of pore bodies in the vertical x direction (the average flow direction). As can be seen in Figs. 1(c) and 1(d), the occupation in the x direction is not continuous because of droplet breakup due to temporal fluctuation in the local pressure. This cartoon is intended to illustrate the maximum height $h_{\max}(j,k)$ that the injected fluid (shown in dark gray) has attained above the point (j,k) in the basal plane. The figure also shows two nearest-neighbor heights (shown in different shades of gray) above $(j+1,k)$ and $(j,k+1)$ as well as the nearest-neighbor height differences. The heights are in units of the lattice spacing, 2.24ℓ, as discussed at the beginning of Sec. II A.

so that $\langle(h_{j,k+1}-h_{j,k})\rangle=\langle(h_{j+1,k}-h_{j,k})\rangle=0$, where the quantities are averaged over all values of (j,k) and over all realizations. For model systems that are $(H=200)\times(W=47)^2$, Fig. 9 shows the number distribution of such single-step (nearest-neighbor) height differences, including both nearest neighbors $\Delta h_1=|(h_{j,k+1}-h_{j,k})|$ and $\Delta h_1=|(h_{j+1,k}-h_{j,k})|$, for viscosity ratio $M=10$. For small height differences, $\Delta h_1<15$, time

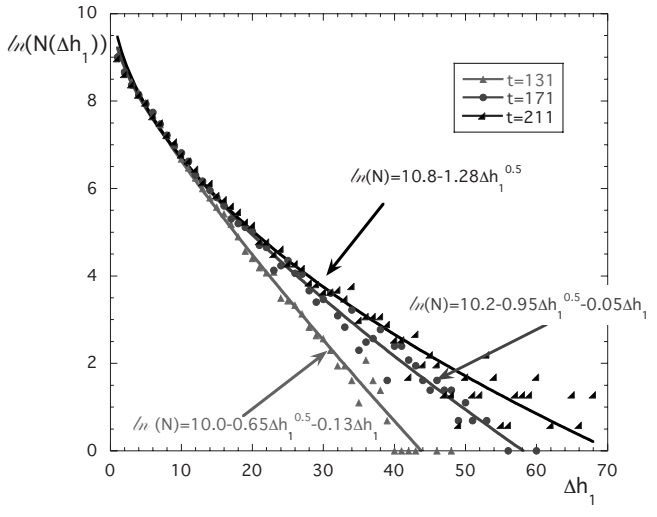

FIG. 9. The number distribution of height differences resulting from a horizontal nn step of unit length 2.24ℓ for $M=1/10$. The fit satisfactorily represents the curvature in the data and exhibits an increasing departure from linearity as time increases. Similar behavior is also observed in the well-past-crossover behavior for $M=1/3$ and $M=1/30$.

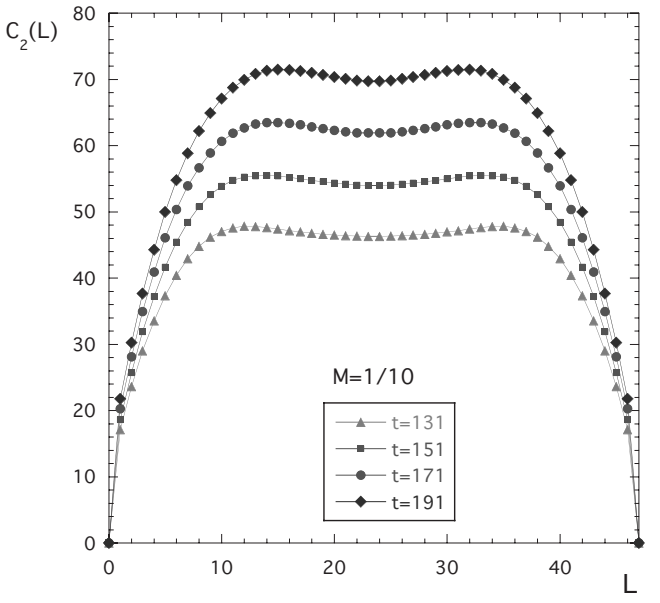

FIG. 10. The correlation function of two heights a distance of L [units of (2.24ℓ)] apart, $C_2(L)$, as in Eq. (11), for the $M=10$ flows in model porous media where $L_{\max}=47(2.24\ell)$.

evolution has negligible effect. However, there is a clear increase in the number of large height differences as time increases, which is obviously consistent with the observed increase in interfacial width with time. Also, this is suggestive of a Lévy flight behavior with occasional large random nearest-neighbor height differences [25–27]. We found that the function,

$$N(\Delta h_1)=N_0 e^{-b\sqrt{\Delta h_1}-c\Delta h_1}, \tag{10}$$

represents a satisfactory fit to the data, with the linear term becoming less important as time increases.

If the interface were self-affine, then different determinations of the roughness exponent should yield the same value. The roughness exponent can be determined from the height-height correlation functions between heights a horizontal distance of L apart, which are defined as

$$C_n(L)=\langle(h_{j,k+L}-h_{j,k})^n+(h_{j+L,k}-h_{j,k})^n\rangle^{1/n}, \tag{11}$$

where the average is over all values of (j,k) and over all realizations [13]. For a self-affine interface, these height-height correlations should all scale as

$$C_n(L)\propto L^{\alpha} \tag{12}$$

for small L, independent of the value of n. In the definition of the height-height correlation function [Eq. (11)], notice that we chose displacements L parallel to the two horizontal axes of the simple-cubic lattice. For $M=10$, the $n=2$ correlation function is shown in Fig. 10.

Because of the symmetry imposed by our periodic boundary conditions, where $h_{j+L_{\max},k}=h_{j,k}=h_{j,k+L_{\max}}$, $L_{\max}$ steps in either direction return to the same point. Therefore $\Sigma_k(h_{j,k+L_{\max}-L}-h_{j,k})^2=\Sigma_k(h_{j,k-L}-h_{j,k})^2=\Sigma_{k'=k-L}(h_{j,k'}-h_{j,k'+L})^2$ so that $C_2(L_{\max}-L)=C_2(-L)=C_2(L)$, explaining the symmetry about the midpoint in Fig. 10.

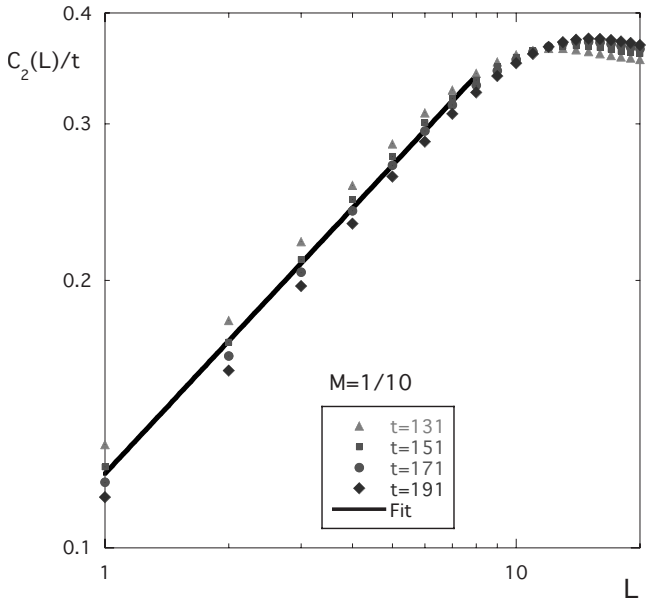

FIG. 11. Power law fit to the small L dependence of the $n=2$ height-height correlations. For analysis purposes, the correlations were normalized by the near linear time dependence of the average interfacial width [i.e., root-mean-square deviations in the height are closely related to the rms height correlations in $C_2(L)$]. For a self-affine interface, the small L behavior should yield the roughness exponent. The straight line shows a power-law fit to the small L data and yields $C_2(L)=0.12L^{0.50}$ so this estimate of the "roughness" exponent has the value, $\alpha=0.50$

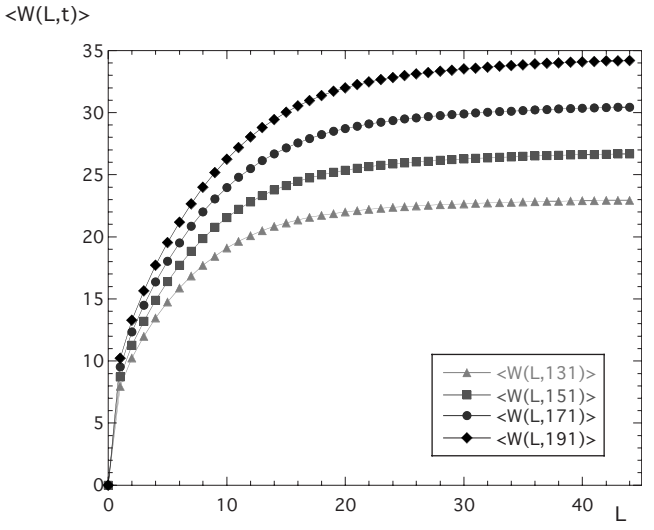

FIG. 12. Averaging the square deviation in the height over all $L\times L$ squares in the system produces the quantity in Eq. (6), $\langle w(t,L)\rangle$, which is plotted vs L for four different well-past-breakthrough times for $M=1/10$ flows.

If the probability of any single step having a height difference $\pm\Delta h_1$ were simply proportional to the $N(\Delta h_1)$ shown in Fig. 10, then the mean-square height difference after L steps, $\langle\Delta h_L^2\rangle$, would be proportional to L, similar to the mean-square length of a random walk, i.e.,

$$\langle\Delta h_L^2\rangle = L\langle\Delta h_1^2\rangle,$$

where $\langle\Delta h_1^2\rangle$ is the mean-square height difference after one horizontal step. Since $\sqrt{\langle\Delta h_L^2\rangle}$ is simply the $n=2$ correlation functions, this random-walk-like assumption predicts the behavior of the $n=2$ height-height correlation function

$$C_2(L) \propto \sqrt{L}, \tag{13}$$

so that the "apparent" roughness exponent should be $\alpha=1/2$. We test this prediction in Fig. 11, where we have collapsed the data in Fig. 10, by assuming that the average height differences increase linearly with time. The partial failure of the collapse of the data, for large L, is still within the uncertainties in our estimate of the growth exponent, $\beta=1.0\pm0.1$. Fitting the small L data for all four times to a power law, the best fit gives $\alpha=0.50$, which is in agreement with our random-walk-like assumptions. However, this is not in agreement with the prediction of the scaling relation, Eq. (7), $\alpha=2-\beta=1.0\pm0.1$ using our value of the growth exponent. In studying the $n=4$ correlation function, we neither have the $\alpha\approx1/2$ nor the $\alpha\approx1$ behavior; rather the exponent is approximately 0.36. This is not consistent with the behavior of a self-affine interface [13], but it is plausible for the random-walk-like assumption, which predicts

$$\langle\Delta h_L^4\rangle = L\langle\Delta h_1^4\rangle + 3L(L-1)\langle\Delta h_1^2\rangle^2, \tag{14}$$

so that $C_4(L)$ would yield an effective exponent between 0.5 and 0.25.

As discussed earlier, the standard method of determining the roughness exponent uses an analysis of $\langle w(t,L)\rangle$ in Eq. (6), i.e., the average of the root-mean-square deviation in the maximum height over an $L\times L$ area perpendicular to the average flow direction [10]. For $M=1/10$, this quantity is shown in Fig. 12. Clearly, there is a small power-law approach to a saturation value, which is the interfacial width (large L limit), as shown in Figs. 5–7 determined by a different method. If, as indicated earlier, the interfacial width grew linearly with time, dividing $\langle w(t,L)\rangle$ by t should collapse the four curves to one. This collapse is shown in Fig. 13. Clearly, there are small deviations from the linear increase in this measure of the interfacial width with time, as was observed earlier. The solid line shows a power-law fit to the small L data. Although the $C_2(L)$ correlations suggested that the "roughness" exponent should be $\alpha=0.50$, this analysis suggests a significantly smaller value $\alpha=0.40\pm0.05$; our determination of the "roughness" exponent from $C_2(L)$, $\alpha=0.50\pm0.02$, is definitely inconsistent with these data.

As mentioned earlier, using the approximate value of the growth exponent $\beta=1$, the scaling relation in Eq. (7) for this system predicts a roughness exponent, $\alpha=1$, which is very different from any of the apparent values of the roughness exponent determined above. Therefore, the evidence suggests that the height differences are not self-affine but are more random-walk-like in that the height differences seem to be randomly distributed. This is qualitatively different from our two-dimensional results where we found agreement with the standard picture. Admittedly our systems have small lateral size so that one might expect that our estimates of the

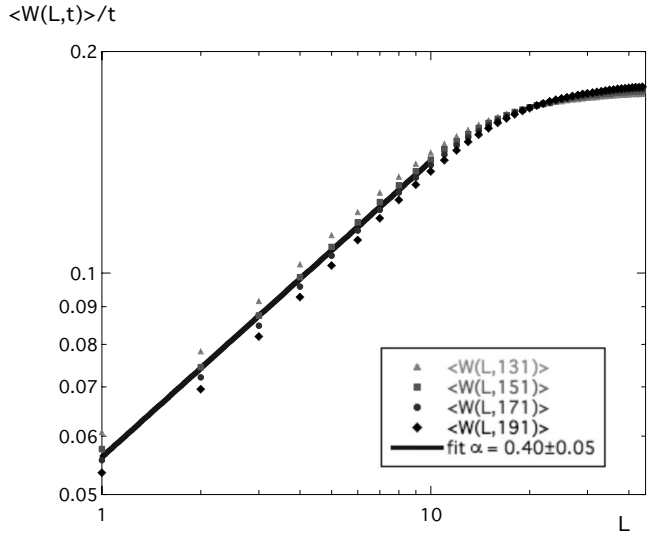

FIG. 13. Normalizing the L-averaged interfacial width, $\langle W(L,t)\rangle$, through dividing by the apparent linear time dependence of the interfacial width, nearly collapses the data to one curve, showing that the linear time dependence of the interfacial width is only approximate. The power-law fit to the small L data is shown by the solid line, which represents the function $0.056L^{0.40}$.

roughness exponents might not be reliable. However, in reviewing our two-dimensional results, we find that the saturation of $\langle w(t,L)\rangle$ occurred for nearly as small a value of L, and those small L results provided a roughness exponent in agreement with the standard picture, Eqs. (6) and (7) [9]. The approximate nature of the estimate of the growth exponent, $\beta=1$, is apparent from Figs. 11 and 13, where the linear time dependence undercorrects for the large distance behavior. It is somewhat less apparent from Fig. 7, where the well-past-crossover behavior is not precisely horizontal. Our estimate of the growth exponent, $\beta=1.0\pm0.1$ is consistent with power-law fits to the well-past-crossover data in Fig. 7, and to the large-L $M=1/10$ data in Figs. 11 and 13 as well as to the corresponding $M=1/3$ data. In addition, our results are inconsistent with standard KPZ theory [10,21].

IV. CONCLUSIONS

In conclusion, we have observed a crossover from fractal viscous fingering to compact behavior at a characteristic crossover time, τ. The same leading singularity in this characteristic time accounts for the viscosity ratio dependence of the center of mass of the injected fluid and of the interfacial width. Although corrections to this leading singularity begin to be significant for the interfacial width for viscosity ratios, $M>1/10$, these corrections do not seem significant for the average position of the injected fluid for viscosity ratios as large as $M=1/3$. As expected, in the well-past-crossover/compact regime, we observe a linear time dependence for the average position of the low viscosity fluid, Fig. 2, which is related to the interfacial position. We also observe that the interfacial width, as determined by two different measures, grows approximately linearly with time (Figs. 7, 11, and 13). Those results suggest that the growth exponent is close to unity, $\beta=1.0\pm0.1$.

Studying the roughness of the interface through the variation in maximum heights achieved by the low viscosity fluid, we found results consistent with a random-walk-like variation in the heights. The number distribution of nn height differences, Δh_1, exhibited an exponential decrease. These distributions also exhibited a clear increase in the magnitude of these nn height differences with time so that, similar to Lévy flights, there would be a low probability of very large nn height differences. If these height differences were strictly random and uncorrelated, then the mean-square change in height over L steps would equal the mean-square nn height difference, $\langle \Delta h_1^2\rangle$, times the number of steps. Therefore, the $n=2$ height-height correlations, $C_2(L)$, would grow as the square root of L, as they did in Fig. 11, consistent with a roughness exponent, $\alpha=1/2$. If the interface were self-affine, then the same roughness exponent would characterize the short-distance small L behavior of the $n=4$ correlations and of the interfacial width, $W(L,t)$, averaged over an $L\times L$ area of the surface; however, the exponents characterizing these small L behaviors were significantly different from both the value $\alpha=1/2$ from analysis of $C_2(L)$ and the scaling value, $\alpha\approx1$, predicted by Eq. (7). Therefore, these results are inconsistent with a self-affine interface and with an effective long-range surface tension smoothing the interface. Furthermore, the behavior of this interface is inconsistent with the standard picture of a rough interface as presented in Eqs. (6) and (7). It is more consistent with a completely random variation in heights as evidenced by the agreement of our results with Eqs. (13) and (14).

ACKNOWLEDGMENTS

M.F. acknowledges the support of the U. S. Department of Energy, Office of Fossil Energy. He also gratefully acknowledges helpful discussions with Alex Hansen and Thomas Ramstad.

[1] J. Nittmann, G. Daccord, and H. E. Stanley, Nature (London) **314**, 141 (1985).
[2] T. A. J. Witten and L. M. Sander, Phys. Rev. Lett. **47**, 1400 (1981).
[3] R. Lenormand, E. Touboul, and C. Zarcone, J. Fluid Mech. **189**, 165 (1988).
[4] P. Meakin, Phys. Rev. A **27**, 1495 (1983).
[5] P. Meakin, in *The Fractal Approach to Heterogeneous Chemistry*, edited by D. Avnir (Wiley, New York, 1989).
[6] P. Meakin, *Fractals, Scaling, and Growth Far From Equilibrium* (Cambridge University Press, Cambridge, 1998).
[7] M. Ferer, J. Gump, and D. H. Smith, Phys. Rev. E **53**, 2502

(1996).
[8] M. Ferer *et al.*, AIChE J. **41**, 749 (1995).
[9] M. Ferer and D. H. Smith, Phys. Rev. E **49**, 4114 (1994).
[10] *Dynamics of Fractal Surfaces*, edited by F. Family and T. Vicsek (World Scientific, Singapore, 1991).
[11] V. K. Horvath, F. Family, and T. Vicsek, J. Phys. A **24**, L25 (1991).
[12] J. Soriano, A. Mercier, R. Planet, A. Hernandez-Machado, M. A. Rodriguez, and J. Ortin, Phys. Rev. Lett. **95**, 104501 (2005).
[13] A. Hansen, G. G. Batrouni, T. Ramstad, and J. Schmittbuhl, Phys. Rev. E **75**, 030102(R) (2007).
[14] C. S. Nolle, B. Koiller, N. Martys, and M. O. Robbins, Phys. Rev. Lett. **71**, 2074 (1993).
[15] T. Ramstad, Ph.D. thesis, Norwegian University of Science and Technology, 2007.
[16] K. J. Måløy *et al.*, Phys. Rev. Lett. **68**, 213 (1992).
[17] T. Ramstad *et al.*, Phys. Rev. E **70**, 036123 (2004).
[18] T. Ramstad, J. Ø. H. Bakke, and A. Hansen, Strength, Fracture and Complexity **3**, 199 (2005).
[19] S. Santucci, K. J. Mraloy, A. Delaplace, J. Mathiesen, A. Hansen, Jan Oistein Haavig Bakke, J. Schmittbuhl, L. Vanel, and P. Ray, Phys. Rev. E **75**, 016104 (2007).
[20] M. Kardar, G. Parisi, and Y. C. Zhang, Phys. Rev. Lett. **56**, 889 (1986).
[21] E. Marinari, A. Pagnani, and G. Parisi, J. Phys. A **33**, 8181 (2000).
[22] P. Meakin, P. Ramanlal, L. M. Sander, and R. C. Ball, Phys. Rev. A **34**, 5091 (1986).
[23] M. Ferer, G. S. Brohmal, and D. H. Smith, Phys. Rev. E **71**, 026303 (2005).
[24] K. Stevenson *et al.*, Physica A **367**, 7 (2006).
[25] P. Lévy, *Théorie de L'addition des Variables Aléatoires* (Gauthier-Villars, Paris, 1937).
[26] T. Solomon, E. Weeks, and H. Swinney, Phys. Rev. Lett. **71**, 3975 (1993).
[27] P. Santini, Phys. Rev. E **61**, 93 (2000).